# A small animal Raman instrument for rapid, wide-area, spectroscopic imaging

Sarah E. Bohndiek[a], Ashwin Wagadarikar[b], Cristina L. Zavaleta[a], Dominique Van de Sompel[a], Ellis Garai[a], Jesse V. Jokerst[a], Siavash Yazdanfar[b], and Sanjiv S. Gambhir[a,1]

[a]Bio-X Program and Department of Radiology, Molecular Imaging Program at Stanford, Stanford University School of Medicine, Stanford, CA 94305; and [b]General Electric Global Research, Niskayuna, NY 12309

Edited* by Michael E. Phelps, University of California, Los Angeles, CA, and approved June 5, 2013 (received for review January 22, 2013)

**Raman spectroscopy, amplified by surface enhanced Raman scattering (SERS) nanoparticles, is a molecular imaging modality with ultra-high sensitivity and the unique ability to multiplex readouts from different molecular targets using a single wavelength of excitation. This approach holds exciting prospects for a range of applications in medicine, including identification and characterization of malignancy during endoscopy and intraoperative image guidance of surgical resection. The development of Raman molecular imaging with SERS nanoparticles is presently limited by long acquisition times, poor spatial resolution, small field of view, and difficulty in animal handling with existing Raman spectroscopy instruments. Our goal is to overcome these limitations by designing a bespoke instrument for Raman molecular imaging in small animals. Here, we present a unique and dedicated small-animal Raman imaging instrument that enables rapid, high-spatial resolution, spectroscopic imaging over a wide field of view (> 6 $cm^2$), with simplified animal handling. Imaging of SERS nanoparticles in small animals demonstrated that this small animal Raman imaging system can detect multiplexed SERS signals in both superficial and deep tissue locations at least an order of magnitude faster than existing systems without compromising sensitivity.**

Raman spectroscopy is a powerful bioanalytical tool based on the inelastic scattering of photons by molecular bonds; as each bond has a characteristic vibrational energy, the spectrum of Raman scatter peaks provides a unique fingerprint for a given sample. In vivo applications previously were limited by the relatively weak Raman effect (fewer than one event per $10^7$ elastic scattering events) and poor depth of penetration (<1 mm). Recently, surface enhanced Raman scattering (SERS) was shown to overcome these limitations, enabling the use of Raman spectroscopy for molecular imaging in small living subjects (1–4).

SERS is a plasmonic effect in which molecules adsorbed on a rough metal surface experience a $>10^6$-fold increase in Raman scatter intensity (5). The SERS enhancement may be exploited in vivo by coating Raman active molecules onto gold nanoparticles (6), which can be engineered to target specific disease markers (7). Advantages of this approach, as opposed to other optical spectroscopy techniques, include a high sensitivity of detection, a low intrinsic background signal, the environmental and optical stability of nanoparticles, and the ability to multiplex signals from different biological targets (6). Therefore, Raman molecular imaging is not only attractive for studies in small animals, it is also being developed for clinical translation through endoscopy and as an intraoperative imaging approach to guide surgical resection (8, 9). Despite the substantial increase in signal afforded by the SERS approach, reports of in vivo Raman imaging using SERS are relatively rare. Expansion of this promising technique currently is limited by the lack of a dedicated Raman spectroscopy instrument specifically optimized for small animal imaging.

Most SERS studies in vivo use adapted Raman microscopy systems, in which a focused laser spot is scanned in two spatial dimensions ($x$ and $y$) over the sample and a spectrum is recorded at each ($x$,$y$) position on a linear (1D) array CCD. Although this approach maximizes the power density at the sample and the sensitivity of spectral detection, it imposes several limitations that have severely affected the wider development of Raman molecular imaging. First, raster scanning a focused laser spot over the sample to acquire spectroscopic images requires prohibitively long acquisition times (>5 h) to cover an area of just a few square centimeters, making whole-body imaging impossible within the limits of permissible anesthesia duration (4, 10). Second, the use of a tightly focused laser spot makes quantification challenging because of signal fluctuations with the contours of the animal. Third, as spatial resolution is traded against scanning time, relatively poor resolution maps (~0.5–1 mm) usually are acquired. Finally, the animal must be translated under the laser spot, which adds undesirable complexity to the experimental design. Although several microscope manufacturers have developed methods to increase scanning speeds and sample coverage, addressing two of these points (e.g., Renishaw inVia Streamline and Horiba SWIFT DuoScan), these instruments still suffer long scan times (e.g., ~1 h for 1 $cm^2$). Furthermore, point-scanning systems that have been reported for wide-area (> 20 $cm^2$) Raman spectroscopic studies of artwork require long scan times because of the small spot size and duration of sample exposure (11).

In addition to point scanning, it also is possible to perform direct, or "global," Raman imaging (10) for in vivo applications (12, 13), in which a wide area (up to 2 $cm^2$) is illuminated and all spatial points of the image are collected simultaneously on a 2D CCD at a single detection wavelength. Global Raman imaging uses a lower power density for illumination, but for in vivo imaging this is not an issue because ultimately we are limited by the American National Standards Institute's laser safety standards (14). Collecting signal from a narrow spectral band, however, sacrifices the rich spectral fingerprint information, possibly reducing detection sensitivity and making both multiplexing and quantification more challenging (13).

To advance the application of Raman spectroscopy in molecular imaging, we designed a unique and dedicated small animal Raman imaging (SARI) instrument. We used a hybrid of the two approaches described above to maximize acquisition speed and spatial resolution, without sacrificing sensitivity or spectral information. Our SARI instrument is a line-scanning system in which a laser line is raster scanned along the $x$ and $y$ axes. A high-sensitivity 2D electron-multiplying CCD (EMCCD) collects both the spatial information for the $y$ axis, parallel to the entrance slit of the spectrometer, and the Raman spectral fingerprint, dispersed perpendicularly. This hybrid method also has been used

Author contributions: S.E.B., A.W., C.L.Z., S.Y., and S.S.G. designed research; S.E.B., C.L.Z., and E.G. performed research; A.W., D.V.d.S., and J.V.J. contributed new reagents/analytic tools; S.E.B. and D.V.d.S. analyzed data; and S.E.B. and S.S.G. wrote the paper.

Conflict of interest statement: A.W and S.Y. are employees of General Electric.

*This Direct Submission article had a prearranged editor.

[1]To whom correspondence should be addressed. E-mail: sgambhir@stanford.edu.

This article contains supporting information online at www.pnas.org/lookup/suppl/doi:10.1073/pnas.1301379110/-/DCSupplemental.



www.pnas.org/cgi/doi/10.1073/pnas.1301379110

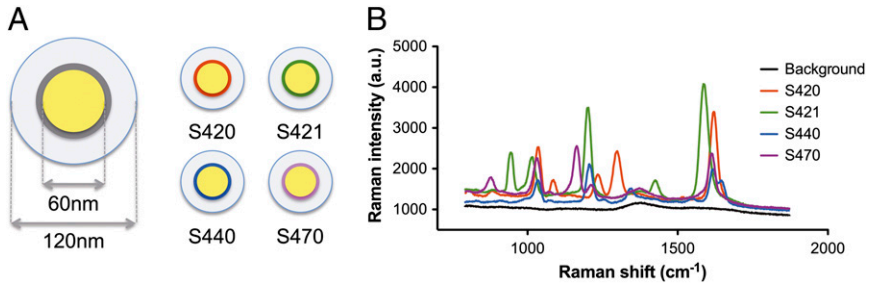


**Fig. 1.** Schematic representation of SERS nanoparticles and their recorded Raman spectra. (*A*) Gold nanoparticles with a 60-nm–diameter gold core are covered with a layer of Raman active material, then a silica coating yielding a particle of 120 nm diameter. The Raman active materials were 4,4′-dipyridyl (S420), d8-4,4′-dipyridyl (S421), *trans*-1,2-bis(4-pyridyl)-ethylene (S440), and 1,2-di(4-pyridyl) acetylene (S470) (4). (*B*) The molecular vibration of the different chemical bonds in the Raman active material after laser excitation at 785 nm yields a unique spectral fingerprint. The background spectrum (free space background) is acquired in the same experimental arrangement without nanoparticles present.

in Raman microscopy and recently was demonstrated as an essential tool for live-cell Raman imaging in vitro (15). In our system, the laser line is scanned rapidly over a stationary sample using 2D galvanometric mirrors, meaning a wide area can be covered

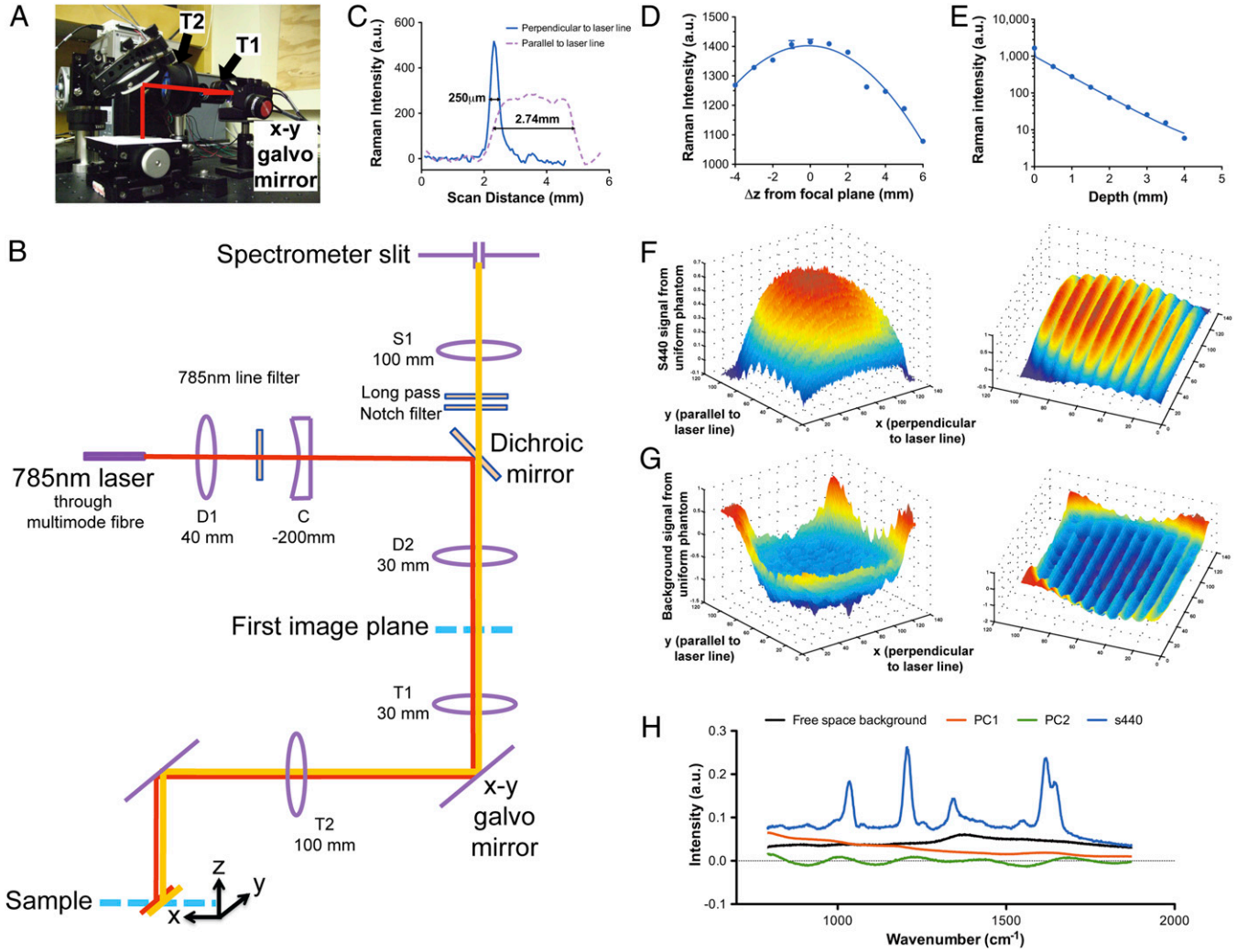


**Fig. 2.** Optical design of SARI system for wide-area line mapping and characterization of performance. (*A*) Photograph of a system with the illumination path overlaid in red. (*B*) Layout of the optical system. (*C*) Line-spread function. Perpendicular to the laser line, the full widths at half-maximum and at tenth-maximum are 250 μm and 675 μm, respectively. (*D*) Raman scatter intensity from S440 SERS nanoparticles as a function of vertical displacement from the focal plane and (*E*) depth in tissue equivalent material. (*F*) System response in the focal plane measured from a full-area (31 × 25-mm) scan of a uniform phantom containing S440 nanoparticles. These data illustrate the Gaussian profile along the laser beam, resulting in lower signal intensity at the edges of the laser line (*y*), and the fall-off in signal intensity at the extreme (*x*,*y*) positions; in both these circumstances, there is an increased signal contribution from the mean free space background (*G*). (*H*) The four principal signal components composing the Raman scatter intensity recorded from the phantom, offset for clarity.

without the need for sample translation. Furthermore, our optical design was optimized specifically to maintain a consistent line profile over a wide area (>6 $cm^2$) to enable small animal imaging.

We demonstrate here that the SARI system enables rapid, high-sensitivity, multiplexed nanoparticle detection in vivo, mapping a large sample area (e.g., a full mouse torso) at least an order of magnitude faster than existing microscopy systems, while maintaining the sensitivity, multiplexing capability, and spectral/spatial resolution necessary for this application.

## Results

**Characterization of SARI System Performance for SERS Nanoparticle Detection.** The four SERS active gold/silica nanoparticle "flavors" used in this work are referred to as S420, S421, S440, and S470; a schematic of their structure and Raman spectra are shown in Fig. 1. The optical design of the SARI system (Fig. 2*A*) is shown in Fig. 2*B*. We first examined the spatial and spectral resolution of the system. The full width at half-maxima (FWHM; Fig. 2*C* and Fig. S1 *A* and *B*) perpendicular (the *x* direction) and parallel to the laser line (the *y* direction) defined the step sizes used for imaging: 250 μm in *x* and 2.5 mm in *y* (to allow some overlap in *y* for stitching of data). The system was relatively insensitive to vertical displacement from the focal plane, up to ±2 mm (Fig. 2*D*). The spectral resolution of the system (Fig. S1 *C* and *D*) was set at 25 $cm^{-1}$. The coefficient of variation of recorded SERS spectra was 1.3% within a single dataset of 50 spectra and 5.4% among five separate datasets (shown in Fig. S2). The collection aperture (Fig. S3) provided sufficient sensitivity to detect SERS signals from S440 nanoparticles at least 4 mm deep in tissue-mimicking material (Fig. 2*E*). The system response across the focal plane (Fig. 2 *F* and *G*) was measured using a uniform phantom containing 24 pM S440 (in a total volume of 28 mL, corresponding to $1.4 \times 10^7$ nanoparticles per cubic millimeter). The spectral contribution from S440 (Fig. 2*H*) fell off significantly toward the outer edges of the field of view, where the contribution of the mean free space background signal (in the absence of any Raman scattering sample) dominated; the S440 contribution was uniform (within 10%) in an area of 18 × 21 $mm^2$. The SARI system demonstrated an excellent limit of detection of just 3.1 pM for S440 in a 5-μL aliquot ($9.3 \times 10^6$ nanoparticles; see Fig. 3*A* for the dilution series).

**Evaluation of In Vivo Multiplexing Capability and Comparison of the SARI System with an Adapted Raman Microscope.** An important validation step in the development of a new instrument is a comparison with a "gold standard" system. We used an adapted Renishaw inVia microscope previously used by our laboratory for in vivo SERS imaging (1, 4) as our gold standard; the adapted microscope demonstrates an exceptional limit of detection due to the higher power density at the sample (Fig. 3*B*). First, we tested the ability of the SARI system to detect single SERS flavors and spectrally unmix components in a living subject, as we demonstrated previously with the inVia system (1, 4). We administered s.c. injections of four separate SERS nanoparticle flavors in the flank of a nude mouse (10 μL of 0.8 nM SERS and of 10 μL Matrigel; total $4.8 \times 10^9$ nanoparticles). To evaluate the multiplexing capability of our instrument, mixtures of the four SERS flavors were injected s.c. on the opposite flank (5 μL of each SERS flavor at 0.8 nM—$2.4 \times 10^9$ nanoparticles—was added to 10 μL of Matrigel in the following combinations: S421 + S440, total 20 μL; S421 + S440 + S470, total 25 μL; S420 + S421 + S440 + S470, total 30 μL). The maps were analyzed with our postprocessing software (*Methods* and *Data Analysis Using a Modified DCLS Algorithm*) to extract the location and intensity of each nanoparticle flavor. The resulting images (Fig. 4*A*) show all four flavors correctly separated into their spectral channels without overlap. Furthermore, the signal intensity observed from each flavor is equivalent, illustrating that the system yields a quantitative signal and, as expected from our characterization results, is relatively insensitive to the surface contours on the flank of the mouse compared with a microscopy system, which exhibits an extremely narrow focus.

We then directly compared the two systems by imaging a single nanoparticle injection site containing 0.8 nM ($2.4 \times 10^9$) S440 SERS nanoparticles, occupying an area of 5 × 5 $mm^2$, with the inVia microscope. In the normal raster scan mode, the estimated scan time on the inVia was prohibitively long (6 h), exceeding the maximum permissible anesthesia duration, hence it could not be completed. We therefore operated the inVia in its "high-speed" Streamline imaging mode (16) with imaging parameters set to achieve comparable spatial and spectral resolution to the SARI system (Fig. 4*B*, *Methods*, and *Renishaw InVia Apparatus and Mode of Operation*). It should be noted that the Renishaw inVia delivers 400-fold higher irradiance in the sample plane compared with the SARI system, as a result of the small size of the laser spot. As it was not practical to adapt our inVia system further to deliver identical irradiance, the inVia spectra showed an improved signal-to-noise ratio for the chosen exposure time (1 s), but this had no impact on the results of our spectral unmixing, hence was not considered to affect our comparison.

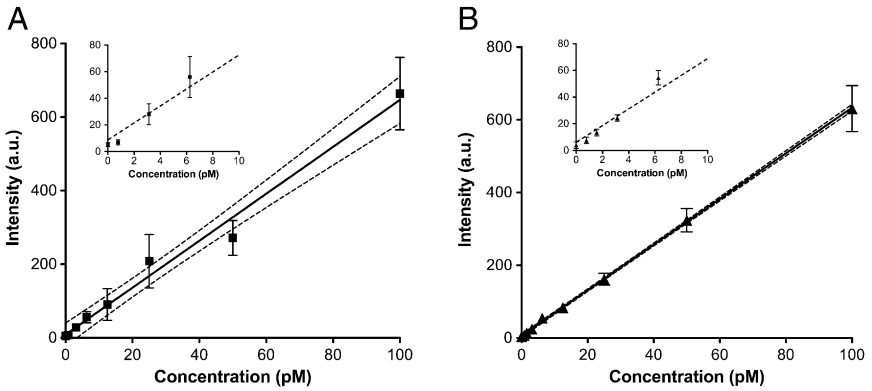


**Fig. 3.** System sensitivity to detection of S440 nanoparticles compared with the Renishaw inVia microscopy system. (*A*) The limit of detection for superficial SERS nanoparticles in our system is 3.1 pM. As expected, the Renishaw microscope, with its 400-fold higher irradiance, has a higher sensitivity, detecting subpicomolar concentrations (*B*). (*Inset*) Close-up of the lowest concentrations, showing that the signal falls into the noise below 3.1 pM on our system but is still linear with concentration at 0.78 pM on the inVia system. Important for quantification purposes, both systems show a linear dependence of recorded Raman scattered intensity with increasing nanoparticle concentration.

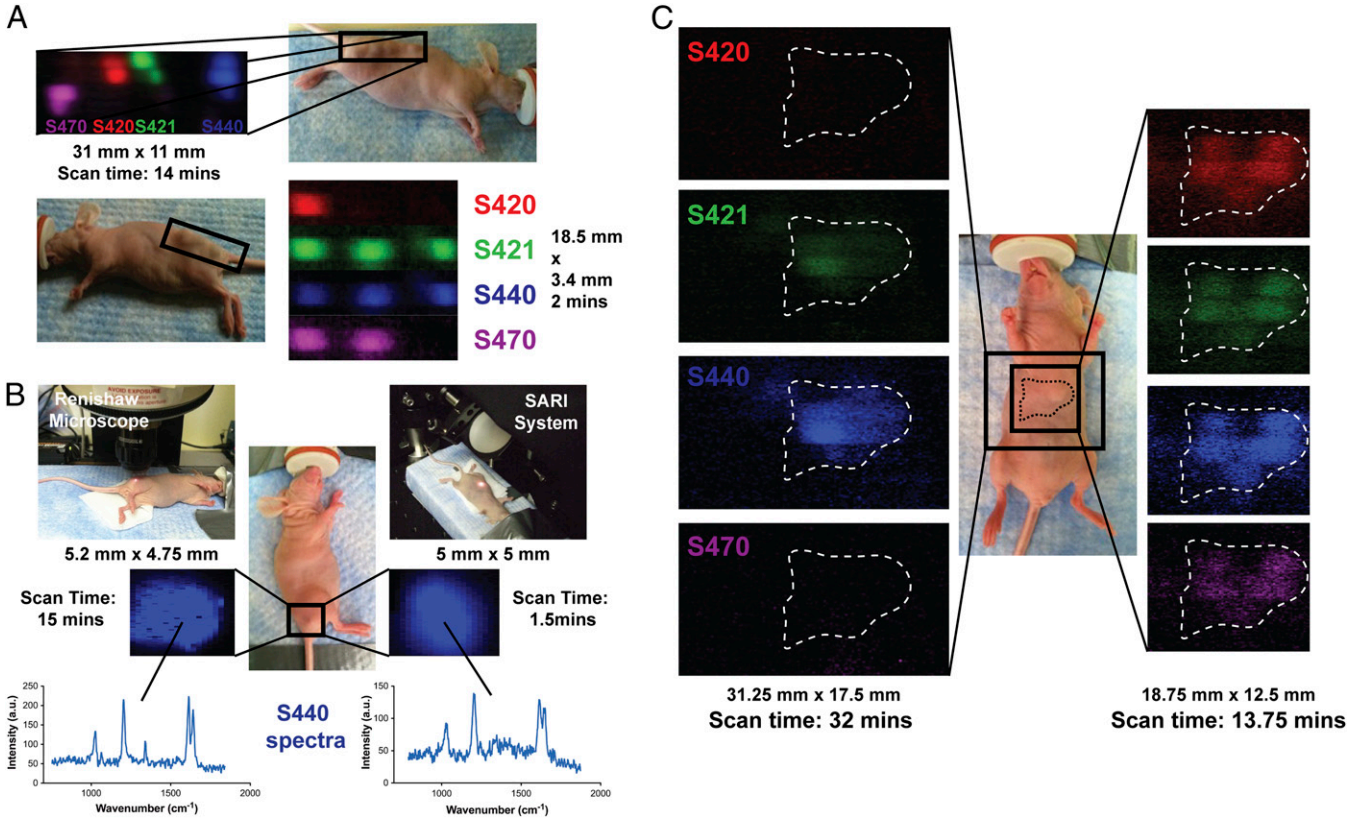


**Fig. 4.** Rapid wide-area imaging of SERS nanoparticle distribution in living mice. (*A*) Subcutaneous injections of SERS nanoparticle flavors, both individual (*Upper*) and multiplexed (*Lower*), were successfully detected and unmixed. The vertical scale is the same in all images. Irregularities in the shapes of these injection sites arise from the curvature of the mouse flank and the stitching of data recorded at different heights. (*B*) Our line-scanning system provides a 3.5-fold improvement in setup time and a 10-fold improvement in scan time compared with the Renishaw inVia microscope operating in the high-speed Streamline mode with matched spectral and spatial resolution. Differences in signal-to-noise ratio in the observed spectra are a result of the higher irradiance provided by the inVia system. (*C*) Mapping of the full mouse torso on our system following i.v. injection of two SERS flavors (S421 + S440, 1 h post injection; *Left*) and a narrower region after injection of four flavors (2 h post injection; *Right*) shows the accumulation of nanoparticles in the liver as expected for clearance through the reticuloendothelial system. The distribution of particles within the different lobes of the liver can be seen to change between these two time points, with greater accumulation in the median and left lobes by 2 h post injection. The vertical scale is the same in all liver images.

In this evaluation, we separately recorded the time to set up the animal and perform the scan. Compared with the Streamline mode, our system gave a 3.5-fold improvement in setup time (6 min vs. 21 min). The inVia requires more careful animal positioning to avoid disconnection of the anesthesia hose during the translation of the animal and also takes a white light "prescan" of the sample area before Streamline imaging. Importantly, we demonstrate a 10-fold improvement in scan time on the SARI system (1.5 min vs. 15 min) compared with the Streamline mode and over 240-fold improvement (1.5 min vs. 360 min) compared with the normal raster scan mode, which represents a significant improvement compared with the existing gold standard.

**Raman Imaging of SERS Nanoparticle Accumulation in Vivo in Deep Tissue.** Finally, to confirm the capability of the system to unmix SERS signals from deeper tissue, we mapped the mouse torso at 1 h and 2 h after tail-vein injection of two (S421 + S440) and four (S420 + S421 + S440 + S470) flavors of SERS nanoparticles (total 200 μL at 0.8 nM; $9.6 \times 10^{10}$ nanoparticles), respectively (Fig. 4*C*). We selected this SERS nanoparticle dose based on previous toxicity studies, in which mice receiving a tail-vein injection of the same dose did not show any adverse changes in vital signs or blood chemistry; although a mild inflammatory response was observed over 24 h, this resolved within 2 wk (9, 17). The nanoparticle dose required for Raman spectroscopy studies is more than an order of magnitude less than that required for other optical imaging modalities, such as photoacoustic tomography, because of the exquisite sensitivity of spectral detection (18).

SERS nanoparticles accumulate in the liver and spleen immediately following injection (9). The SARI system could map the entire mouse torso ($31.25 \times 17.5$ mm$^2$) in 30 min and correctly identify S421 and S440 as the flavors contributing to the signal localized within the liver. Furthermore, a narrower region ($18.75 \times 12.5$ mm$^2$) focused on the liver after injection of four flavors was mapped in under 15 min, and the resulting image correctly separated the four flavors into their spectral channels with equal intensities, reflecting their equal concentrations in the injection. This encouraging demonstration of quantitative, deep tissue multiplexing shows that our system has the potential to advance SERS-based Raman spectroscopy as a molecular imaging technique.

## Discussion

Raman spectroscopy, amplified by SERS nanoparticles, is a noninvasive molecular imaging modality with ultra-high sensitivity. The optical and environmental stability of the SERS nanoparticles, together with the unique ability to multiplex readouts from different molecular targets using a single excitation wavelength, makes Raman molecular imaging an exciting tool with many possible medical applications, such as characterizing newly diagnosed malignancy and guiding surgical resection (7, 8). The use of

adapted Raman microscopes in the preclinical setting currently is a key factor restricting the wider development of Raman spectroscopy as a molecular imaging technique, because of slow acquisition times, small imaging areas, poor spatial resolution, and practical limitations in animal handling. The combination of these factors makes preclinical validation of SERS nanoparticles extremely challenging.

We have demonstrated here a dedicated system for small animal Raman imaging. The SARI system achieved at least an order-of-magnitude improvement in scan time compared with our gold standard Raman microscope operating in Streamline mode, and was more than two orders faster than the expected raster scan time. Our system could image a wide area of 31 × 25 mm (>6 $cm^2$) without needing to move the animal (giving a 3.5-fold improvement in animal setup time). This field of view was imaged with a spatial resolution of 250 × 64 μm and full area coverage in under 30 min, whereas an area of 1 $cm^2$ could be scanned in just 6 min. Our depth of field was sufficient to provide a quantitative readout of SERS nanoparticle concentration in tissue and was not affected by the contours of the mouse surface. Importantly, we also could detect SERS nanoparticle accumulation in deeper tissue, up to 4 mm below the surface.

In addition to the potential for small animal imaging, the high-throughput nature of our system (e.g., 5 × 5 $mm^2$ in 1.5 min) might provide an avenue to perform assays of targeted nanoparticle binding and retention following incubation with cells (Fig. S4). At present, the efficiency of targeting is tested first in high-throughput assays with cells in situ by tagging the nanoparticle with a fluorescent dye before proceeding to Raman experiments (7). Our system provides a means to rapidly assess a panel of targeted SERS nanoparticles—for example, in a multiwell plate—directly using the Raman signals. The limited spatial resolution, however, means that single-cell imaging with promising candidates still would have to be performed on a microscopy system to determine subcellular localization of the SERS signal.

Although the SARI system offers clear advantages over an adapted microscope, several improvements still may be made in a second-generation instrument. The working distance of the system, despite being longer than that of microscopy systems, is still limited to within a few millimeters of the focal plane (Fig. 2*D*) because of the multimode optical fiber output of the laser, which degrades the spatial quality of the beam. Upgrading to a collinear design with a single-mode laser would improve the range of working distance and account for variations in sample height that would be encountered when imaging a whole mouse, rather than just the torso. Improvements in sensitivity without increasing irradiance also will be possible in the near future, given the current pace of developments in spectrometer–detector technologies.

The depth of penetration of the system is also limited to <4 mm (Fig. 2*E*). At present, the maximum reported depth of penetration using the spatially offset Raman spectroscopy (SORS) method is 45–50 mm (19), which is sufficient for imaging in small animals, and the depth using Raman tomography is 27 mm (20). Although this depth is limited with respect to hybrid optical modalities such as photoacoustic imaging (18), Raman spectroscopy requires a dose of nanoparticles an order of magnitude lower to generate a detectable signal (8, 18, 21) and enables multiplexed readout with only a single wavelength of excitation (4), simplifying the instrumentation considerably. Incorporating the SORS technique into a future generation of this system should improve our available depth of penetration.

In summary, we have designed, characterized, and applied a dedicated small animal Raman imaging instrument capable of rapid, wide-area detection of multiplexed SERS nanoparticles in living mice. The SARI approach should enable Raman spectroscopy to advance rapidly as a molecular imaging tool for small animal studies, such as the in vivo characterization of uptake dynamics for different nanoparticle designs, with a range of targeting moieties that were not possible in the past. This in turn might accelerate efforts directed toward clinical translation of SERS strategies for applications including endoscopy and intraoperative imaging.

## Methods

**Optical Design.** The system consists of an optical assembly for laser excitation and Raman signal collection that was coupled to the entrance slit of a spectrometer (Fig. 1*A*). The laser excitation was provided by a 785-nm, narrow-line width (<50:00 pm) source (MiniLite; BaySpec). The laser was fiber coupled to external optics using a 105-μm multimode fiber and delivered up to 290 mW output power in the focal plane. The Raman signal collection was performed with a Czerny–Turner spectrometer [focal length (f) = 303 mm; Shamrock 303i; Andor] integrated with an EMCCD with extended red quantum efficiency for improved response in the near-infrared (Luca 604 EMCCD; Andor).

**Illumination Pathway.** The laser excitation path is indicated by the red line in Fig. 2*B*. Laser light from the multimode fiber was shaped to form a 1,200 × 75-μm line at the first image plane using a combination of the laser line coated plano-convex lens D1 [diameter (d) = 25 mm, f = 40 mm; NT69-497; Edmund Optics], the plano-concave cylindrical lens C (d = 25.4 mm, f = −200 mm; LK1069RM-B; Thorlabs), and an NIR achromat, D2 (d = 25.4 mm, f = 30 mm; AC254-030-B; Thorlabs). The laser line filter (LL01-785-12.5; Semrock) was placed after D1 to remove stray fluorescence from the optical fiber. The dichroic beamsplitter (LPD01-785RU-25; Semrock) reflected the laser beam to the first image plane. The line defined in the first image plane was magnified to form a 2,810 × 250-μm line (Fig. S1 *A* and *B*) in the sample plane using a combination of the achromatic lenses T1 and T2 [d = 25.4 mm, f = 30 mm (AC-254–030-B) and d = 50.8 mm, f = 100 mm (AC508-100-B); Thorlabs). A two-axis galvanometric mirror assembly (d = 10 mm; GVS012; Thorlabs) placed between T1 and T2 allowed the laser line to be scanned in the sample plane over a 31.25 × 25-mm area and was calibrated to move at 3.125 mm/V.

**Imaging Pathway.** The path traversed by the light emitted by the sample (SERS + autofluorescence signal) to the spectrometer slit is indicated by the orange line in Fig. 2*B*. The light emitted along the line on the sample was imaged in the first image plane through T1, the galvo mirrors, and T2. The combination of D2 and the achromat S1 (d = 25.4 mm, f = 100 mm; AC254-100-B; Thorlabs) imaged the line onto the spectrometer slit through the dichroic mirror, which transmits wavelengths beyond 795 nm with over 90% efficiency. All lenses in the light collection path were achromats to minimize chromatic aberration of the broadband emitted light. The F-number of lens S1 was matched to the spectrometer (F/4) to avoid light losses. A single-notch filter (bandwidth = 39 nm; NF03-785E-25; Semrock) and a long-pass edge filter (LP02-785RE-25; Semrock) were used to remove any residual 785-nm laser light and to ensure that only the Stokes-shifted emission light passed through the spectrometer slit.

**Data Acquisition and Control.** To match the desired wavenumber range of the SERS nanoparticles, the spectrometer was operated at a 300-line pairs/mm grating blazed at 1,000 nm. Given a nominal dispersion of 10.43 nm/mm and an 8-mm–wide sensor, this produces a spectral range of 83 nm. With excitation at 785 nm, a dispersion range of 828–911 nm corresponded to a wavenumber range of 665–1,771 $cm^{-1}$. The galvo mirrors, spectrometer, and EMCCD settings were controlled through a LabVIEW interface (National Instruments) on the control PC. The galvo mirrors moved the laser line across the sample area in steps of 250 μm in *x* (perpendicular to the length of the laser line) and 2.5 mm in *y* (parallel to the line) to allow some overlap of positions for image stitching. The step size in the *x* direction was determined by the width of the laser line in that dimension (Fig. 2*C* and Fig. S1*B*). The 2D image frame from the EMCCD at each position recorded the spatial dispersion along the laser line in one dimension and the spectral dispersion of the Raman scattered photons along the other.

**System Optimization.** To maximize the sensitivity of the system for detecting SERS nanoparticles while maintaining a fast collection time and adequate spectral resolution, the following parameter settings were used. First, the EMCCD was operated at maximum gain (200) and the exposure time was set at 1 s, although this could be adjusted depending on the signal-to-noise ratio obtained from a given sample. In all experiments, the slit width was set to

110 μm (Fig. S1*C*). All measurements were performed using a laser current of 1.4 A, corresponding to a power of 290 mW in the sample plane. The background signal with no sample in place was recorded for the entire imaging range and averaged to give a mean free space background spectrum (see Fig. 2*H* and *Data Analysis Using a Modified DCLS Algorithm*).

**Data Analysis and Statistics.** Quantitative Raman spectral analysis was performed for all experiments using a modified direct classical least-squares (DCLS) method. The reported Raman intensity in this work is the weight of the associated nanoparticle flavor calculated by the modified DCLS procedure. The Raman spectral analysis and rebinning procedure was performed in MATLAB (MathWorks). For further details on the DCLS modification, see *SI Text*.

**SERS Nanoparticles.** SERS active nanoparticles (Cabot Security Systems, formerly Oxonica Materials Inc.) consisted of a 60-nm–diameter gold core covered with a layer of Raman active material and a silica coating, making the final diameter 120 nm. The Raman active material varied for each of the four SERS particles used in this study, referred to as S420, S421, S440, and S470 (Fig. 1). S440 was used for all single-particle and characterization studies.

**System Characterization.** ***Reference spectra and sensitivity measurements.*** All nanoparticles were studied in 5-μL aliquots placed on Parafilm and mounted on a quartz slide. The diameter of the 5-μL droplet was sufficient to remain within the length of the laser line, and Raman data were acquired by scanning in the *x* direction alone. The quartz slide prevented contamination of the Raman spectra with extraneous peaks. For the reference spectra measurements, a concentration of 0.8 nM was used for each nanoparticle flavor. For the sensitivity measurements, a dilution series of S440 nanoparticles was made using MES buffer at pH 7, starting from a concentration of 100 pM and performing 1:2 dilutions down to 0.78 pM.

***Edge-spread function.*** A sharp edge printed in blue ink was used to determine the limiting scanning resolution of the system. The laser line was scanned with the edge perpendicular to the *x* and *y* directions. The resulting edge-spread function was differentiated to obtain the line-spread function, from which the FWHM of the laser line was determined. These measurements (Fig. 2*C*) compared favorably with those made independently by directly imaging the laser line (Fig. S1 *A* and *B*).

***Depth of field.*** A 5-μL aliquot of S440 nanoparticles at 100 pM was placed on Parafilm on a quartz slide in the center of the *x*–*y* plane and scanned using a translating post (PH3T; Thorlabs) in 1-mm steps through the calculated focal plane. The SERS intensity was plotted as a function of position and a parabola fitted to determine the peak signal and hence the focal plane.

***Depth of penetration.*** The maximum imaging depth for SERS nanoparticles was determined using a tissue-mimicking phantom. The tissue-mimicking background material was prepared using a combination of lipid (Liposyn II 10%; Hospira) and India ink in distilled water containing agarose (16500-500; Invitrogen) and allowed to set. The final concentration was 1% lipid, 0.04% India ink, and 1% agarose, giving an absorbance of 0.1 $mm^{-1}$. A solution of S440 (0.5 nM) in 1% agarose was then poured into a well in the center of the phantom and allowed to set. The phantom was positioned with the nanoparticle inclusion at the center of the focal plane. The Raman scatter intensity was recorded as the phantom was covered in 0.5-mm depth increments with tissue-mimicking fluid (as above without agarose) until the S440 signal no longer could be distinguished from the background. The S440 intensity then was plotted as a function of depth and fit to an exponential decay.

***Response uniformity in the focal plane.*** The uniform phantom contained S440 nanoparticles (24 pM) in 1% agarose; an identical background phantom contained no nanoparticles. Data were acquired from both phantoms over the full range of the galvo mirrors. Principal component analysis was performed on the two datasets. Most of the variance was explained by the first four principal components. The weights of the S440 signal and the mean free space background in the DCLS analysis from the two phantoms then were used to assess the response uniformity in the *x*–*y* plane.

**Animal Imaging.** Female nude mice (6–8 wk, Charles River) were used for Raman spectroscopic imaging studies. All procedures performed on animals were approved by Stanford University's Institutional Animal Care and Use Committee and were within the guidelines of humane care of laboratory animals. Anesthesia was maintained through inhaled isoflurane. Subcutaneous nanoparticle injections consisted of a 1:1 ratio of SERS nanoparticles to Matrigel, a gelatinous protein formulation that resembles the complex extracellular environment found in tissues. Matrigel was used to prevent the SERS nanoparticles from diffusing out of the skin. Nanoparticles administered through the tail vein were suspended in MES buffer. The speed of our system was compared with the Renishaw inVia Raman microscope. The fastest imaging measurement on the Renishaw microscope is the Streamline imaging mode, which uses charge movement along the spatial dimension of the CCD detector to perform dynamic line scanning as the sample is moved under the laser point focus in the *x*–*y* plane. See *SI Text* for more details on the operation of the Renishaw microscope.

**ACKNOWLEDGMENTS.** We thank Dr. Steve Sensarn for helpful discussions on system development. This research is funded by the Center for Cancer Nanotechnology Excellence and Translation through a National Cancer Institute–National Institutes of Health U54 Grant (1 U54-CA151459).

1. Keren S, et al. (2008) Noninvasive molecular imaging of small living subjects using Raman spectroscopy. *Proc Natl Acad Sci USA* 105(15):5844–5849.
2. Qian X, et al. (2008) In vivo tumor targeting and spectroscopic detection with surface-enhanced Raman nanoparticle tags. *Nat Biotechnol* 26(1):83–90.
3. Samanta A, et al. (2011) Ultrasensitive near-infrared Raman reporters for SERS-based in vivo cancer detection. *Angew Chem Int Ed Engl* 50(27):6089–6092.
4. Zavaleta CL, et al. (2009) Multiplexed imaging of surface enhanced Raman scattering nanotags in living mice using noninvasive Raman spectroscopy. *Proc Natl Acad Sci USA* 106(32):13511–13516.
5. Wachsmann-Hogiu S, Weeks T, Huser T (2009) Chemical analysis in vivo and in vitro by Raman spectroscopy—from single cells to humans. *Curr Opin Biotechnol* 20(1):63–73.
6. Doering WE, Piotti ME, Natan MJ, Freeman RG (2007) SERS as a foundation for nanoscale, optically detected biological labels. *Adv Mater* 19(20):3100–3108.
7. Jokerst JV, Miao Z, Zavaleta C, Cheng Z, Gambhir SS (2011) Affibody-functionalized gold-silica nanoparticles for Raman molecular imaging of the epidermal growth factor receptor. *Small* 7(5):625–633.
8. Kircher MF, et al. (2012) A brain tumor molecular imaging strategy using a new triple-modality MRI-photoacoustic-Raman nanoparticle. *Nat Med* 18(5):829–834.
9. Zavaleta CL, et al. (2011) Preclinical evaluation of Raman nanoparticle biodistribution for their potential use in clinical endoscopy imaging. *Small* 7(15):2232–2240.
10. Schlücker S, Schaeberle MD, Huffman SW, Levin IW (2003) Raman microspectroscopy: A comparison of point, line, and wide-field imaging methodologies. *Anal Chem* 75(16):4312–4318.
11. Brambilla A, et al. (2011) A remote scanning Raman spectrometer for in situ measurements of works of art. *Rev Sci Instrum* 82(6):063109.
12. Mallia RJ, McVeigh PZ, Veilleux I, Wilson BC (2012) Filter-based method for background removal in high-sensitivity wide-field-surface-enhanced Raman scattering imaging in vivo. *J Biomed Opt* 17(7):076017.
13. McVeigh PZ, Mallia RJ, Veilleux I, Wilson BC (2013) Widefield quantitative multiplex surface enhanced Raman scattering imaging in vivo. *J Biomed Opt* 18(4): 046011.
14. American National Standards Institute Inc. (2007) *American National Standard for Safe Use of Lasers* (Laser Institute of America, Orlando, FL), ANSI Z136.1–2007, revision of ANSI Z136.1-2000.
15. Palonpon AF, et al. (2013) Raman and SERS microscopy for molecular imaging of live cells. *Nat Protoc* 8(4):677–692.
16. Bernard S, Beyssac O, Benzerara K (2008) Raman mapping using advanced line-scanning systems: Geological applications. *Appl Spectrosc* 62(11):1180–1188.
17. Thakor AS, et al. (2011) The fate and toxicity of Raman-active silica-gold nanoparticles in mice. *Sci Transl Med* 3(79):79ra33.
18. Ntziachristos V (2010) Going deeper than microscopy: The optical imaging frontier in biology. *Nat Methods* 7(8):603–614.
19. Stone N, et al. (2011) Surface enhanced spatially offset Raman spectroscopic (SESORS) imaging—the next dimension. *Chem Sci* 2(4):776–780.
20. Demers JL, Davis SC, Pogue BW, Morris MD (2012) Multichannel diffuse optical Raman tomography for bone characterization in vivo: A phantom study. *Biomed Opt Express* 3(9):2299–2305.
21. James ML, Gambhir SS (2012) A molecular imaging primer: Modalities, imaging agents, and applications. *Physiol Rev* 92(2):897–965.